Single Molecule Magnets of Co$_2$ and Co$_2$La MOFs Synthesized by New Schiff Base Ligand N,N′-bis(o-Vanillinidene) Ethylenediamine (o-VEDH$_2$)

Mithun Kumar Ghosh [1†], Barun Jana [2*†] and Tanmay Kumar Ghorai [1,3*†]

[1] Nanomaterials and Crystal Designing Laboratory, Department of Chemistry Indira Gandhi National Tribal University, Amarkantak, India, [2] Department of Chemistry, Malaviya National Institute of Technology, Jaipur, India, [3] Nanomaterials and Crystal Designing Laboratory, Department of Chemistry, Guru Ghasidas Vishwavidyalaya, Bilaspur, India

Schiff base ligand N,N′-bis(o-vanillinidene) ethylenediamine (o-VEDH$_2$) has been employed to synthesize new $[Co^{II}Co^{IV}(o\text{-VED})(OAc)_2(\mu_2\text{-OAc})(OMe)]\bullet MeOH$ (**1**) and $[Co_2^{IV}(o\text{-VED})_2(en)_2(NCCH_3)(OCH_3)][La(NO_3)_6](NO_3^-)\bullet 2MeOH\bullet MeCN\bullet H_2O$ (**2**) metal–organic frameworks (MOFs) that have interesting single molecule magnets (SMMs) property. The synthesized complexes are characterized by single crystal X-ray diffraction, fourier transform infrared spectroscopy (FTIR), UV-visible spectroscopy, and squid magnetic measurement. Single crystal X-ray data show that both complexes crystallize in the monoclinic crystal system with $P2_1/c(14)$ and $P2_1/n(14)$ space groups and generate unique MOF-like structures. Overall, both the metal centers of **1** form octahedral geometry with a butterfly core structure. Variable temperature (T) and field (H) solid-state direct-current (dc) and alternative current (ac) magnetic susceptibility measurements were performed on both the complexes over 1.8 to 300 K, which exhibited a ground state spins (S) of 4 and 5 of complexes **1** and **2**, respectively. The AC out-phase and in-phase properties of complexes show SMMs. Other properties such as optical, sensing, and DNA-binding interactions were also investigated by the complexes. Complexes **1** and **2** have energy band gaps of 3.7 and 3.03 eV indicating semiconductor properties. Simultaneously, complex **1** was found to sense H$_2$O$_2$ with a rate constant (k) = 1.59 × 10^{-4} s^{-1}, whereas complex **2** was found to bind with calf-thymus–DNA by intercalation mode with binding constant (K_b) of 1.22 × 10^5 M^{-1}.

Keywords: synthesis, schiff base, MOFs, SMMs, sensing and CT-DNA 3

INTRODUCTION

In the last few years, multifunctional homo/pseudoheterometallic metal–organic frameworks (MOFs) showing distinct physical properties have been reported not only for the basic intensive research but also for their potential applications in new technologies (Yang et al., 2015; Zhang et al., 2016; Clough et al., 2017; Dong et al., 2017; Long, 2019; Qi et al., 2019). In material science, multifunctional metal complexes having magnetomolecular properties are of interest because

they found potential applications in the field of sensors and biology (Chelebaeva et al., 2009; Montgomery et al., 2009; Yuan et al., 2018). In recent literatures, different groups have reported the syntheses of different bimetallic complexes with bifunctional magnetomaterial properties (Freitas et al., 2010; Kumar et al., 2019; Wu et al., 2019). Here, the magnetic properties of single molecules are of interest, and significant amount of results is available (Sessoli et al., 1993; Gatteschi and Sessoli, 2003; Tasiopoulos et al., 2004; Bogani and Wernsdorfer, 2010; Van Slageren, 2011; Vincent et al., 2012; Wu et al., 2019). The chemistry of single molecule magnets (SMMs) was started through the discovery of Mn$_{12}$Ac in 1993. It was found that large ground state spin (S) and negative zero field splitting (D) are the two essential factors that determine SMMs properties (Sessoli et al., 1993; Gatteschi and Sessoli, 2003; Tasiopoulos et al., 2004; Bogani and Wernsdorfer, 2010; Van Slageren, 2011; Vincent et al., 2012; Wu et al., 2019). In this regard, syntheses of lanthanide-based SMMs are quite of interest because of their various potential applications in high-density storage, quantum computers, and spintronics devices (Sessoli et al., 1993; Ishikawa et al., 2003; King et al., 2005; Tang and Zhang, 2015; Ding et al., 2016). Along with this, the mixed cobalt and lanthanide complexes with Schiff based ligands are also of significant interest because of their SMMs properties (Gupta et al., 2016; Modak et al., 2016). At the same time, metal complexes of Schiff base ligands are also of huge importance in the field of medicinal and pharmaceutical chemistry due to their antibacterial (Woodruff et al., 2013), antifungal (Lv et al., 2006), and antitumor activities (Alghool et al., 2013) and DNA-binding (Yang et al., 2000) properties. Effective anticancer drugs generally have an active site that mainly binds to the cancer cell's DNA and reduces cancer cell activity, which lead to death of the cells (Wang et al., 2006, 2011; Pathak et al., 2018). Medicines that are used to prevent cancer from interacting with DNA through electrostatic, intercalative, or groove binding depend on binding methods of anticancer drugs (Zuber et al., 1998; Li et al., 2010; Pages et al., 2015; Zeng et al., 2017). In the past few years, researchers have reported cobalt and lanthanum complexes of Schiff base ligands and investigated their calf-thymus (CT)–DNA binding (Yang et al., 2006; Santini et al., 2013; Wang et al., 2014).

In the biological field, it is well-known that reactive oxygen species (ROS) and reactive nitrogen species play a significant role in the development of cancer cells in the human body. ROS such as superoxide anion (O$_2^{\bullet-}$) and hydroxyl radical ($\bullet$OH) are generally generated during the decomposition of hydrogen peroxide, which is the main reason for cancer cell generation (Tredwin et al., 2006; Shahabadi et al., 2010; Zhao et al., 2012). The development of practical and accurate H$_2$O$_2$ detection techniques is therefore necessary to ensure improved healthcare. Last few years, scientists have developed lanthanide/transition metal–based MOFs and investigated their different sensing activity (Droge, 2002; Gao et al., 2016; Koo et al., 2016; Zeng et al., 2016). Herein, we report the H$_2$O$_2$-sensing activity of Co-MOFs.

Our research group focused on the synthesis of magnetomolecular materials that have multifunctional applications. Recently, we have reported magnetomolecular Cu$_3$ 1D polymer and Mn$_{12}$ benzoate cluster that have multifunctional
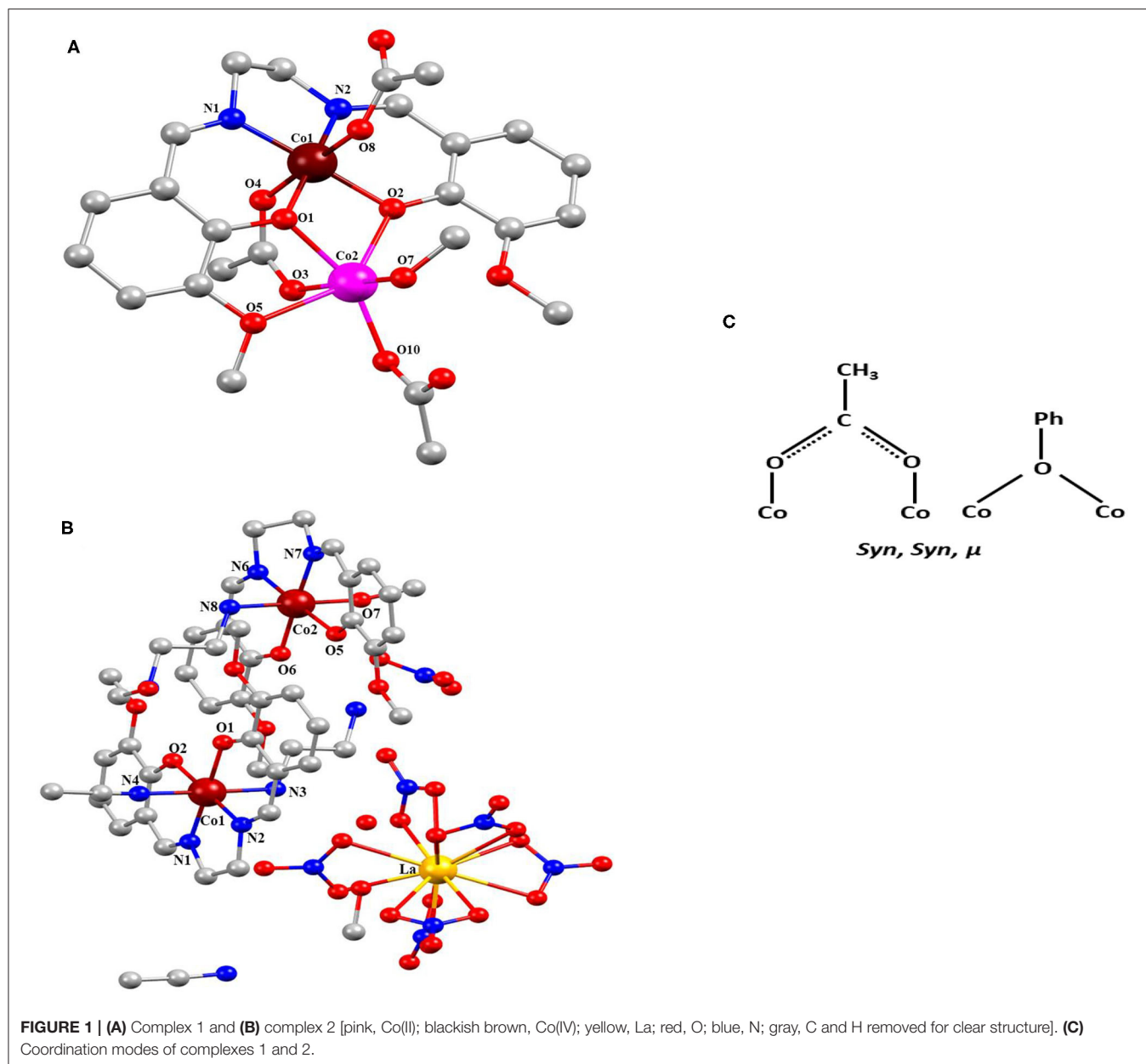
applications such as antibacterial, anticancer, antioxidant, cytotoxicity, and magnetic (Mandal et al., 2017; Pathak et al., 2019). From the literature examples, it is clear that multifunctional homometallic Co/Co or pseudoheterometallic Co/La clusters might show properties relevant to sensing, biological, and magnetic properties. Herein, we report two new homometallic and pseudoheterometallic Co and Co-La–based metal clusters along with their SMMs, optical, sensing, and DNA-binding interaction properties.

RESULTS AND DISCUSSIONS

For the synthesis of pseudoheterometallic Co/La metal cluster, we have chosen the simple N,N′-bis(o-vanillinidene) ethylenediamine (o-VEDH$_2$) as our ligand system. Here, the presence of two different bonding atoms (O, N) may preferentially choose one above the other between Co and La, and that may result in the formation of our desired product. Accordingly, we have reacted to the readily synthesized (o-VEDH$_2$) with a mixture of La(NO$_3$)$_3$·6H$_2$O and Co(NO$_3$)$_2$·6H$_2$O in methanol in 2:1:1 ratio. Subsequent work and crystallization resulted in the formation of black crystals. Elemental analysis and infrared spectroscopy indicated the formation of the pseudoheterometallic cluster (**2**). Determination of molecular structure via single crystal X-ray diffraction further confirmed the formation of a pseudoheterometallic Co/La metal cluster. For comparison purposes, we have also decided to synthesize a homometallic Co/Co molecular cluster via a 1:2 reaction of (o-VEDH$_2$) and Co(OAc)$_2$ in methanol. In this case, subsequent workup also led to the isolation of black crystals. Initial characterization utilizing elemental analysis and infrared spectroscopic data indicated the formation of a homometallic bis-Co cluster (**1**). The molecular geometry of cluster **1** was established via a single crystal X-ray diffraction study.

Structural Description

Complexes **1** and **2** are crystalized in the monoclinic system with P2$_1$/c and P2$_1$/n. **Figure 1** shows molecular structures of **1** and **2**. Crystal data and selected bond distances and angles are summarized in **Tables 1**, **2**, respectively. In complex 1, two cobalt atoms are residing in two different electronic environments and surrounded by one o-VED ligand moiety, coordinated through both the oxygen and nitrogen atom, and OAc$^-$ anions either through μ_2 or μ_3 coordination mode. Both o-VED ligand nitrogen (N1 and N2), coordinated with the Co1 atom and o-VED's two hydroxo-oxygen (O1 and O2) bridged with both the Co1 and Co2. Further, one of the acetate anions (O3 and O4) bridges both the Co atoms in a μ_2 coordination mode. The octahedral coordination geometry of the two Co atoms has been achieved by the addition of terminally connected acetate groups via O8 and O10, respectively. Overall, both the metal centers form octahedral geometry with a butterfly core structure. The distance between Co1 and Co2 is 3.043(19) Å, which is relatively long for any covalent interaction among them. Interestingly, the average bond distance from Co1 to its two coordinating nitrogen atoms is 1.866 Å, whereas the average bond distance

FIGURE 1 | (A) Complex 1 and **(B)** complex 2 [pink, Co(II); blackish brown, Co(IV); yellow, La; red, O; blue, N; gray, C and H removed for clear structure]. **(C)** Coordination modes of complexes 1 and 2.

to its four coordinating oxygen atoms is 1.902 Å. Relatively short bond distances between Co-O and Co-N indicate that the Co atom may be present in +4 oxidation state. On the other hand, the average bond distance from Co2 atom to its six coordination oxygen atoms is 2.079Å. Relatively higher Co-O bond lengths indicate that the Co2 present in a lower oxidation state as compared to Co1. Literature references indicate that in this case, Co2 may present in +2 oxidation state. Interestingly, complex **2** is a double salt of Co$_2$ and La fragments. In complex **2**, both the Co atoms are coordinated to two separate *o*-VED moieties through their oxygen atoms (O$_1$ and O$_2$ to Co$_1$; O$_5$ and O$_6$ to Co$_2$) and nitrogen atoms (N1 and N2 to Co1; N6 and N7 to Co2). In addition to this, both the central cobalt atoms are terminally coordinated to two different ethylene diamine

groups through one of the nitrogen of –NH$_2$ groups (N3 to Co1 and N8 to Co2). The octahedral coordination sphere of Co1 is completed via coordination of an additional acetonitrile group (N4), whereas the octahedral coordination of Co2 gets fulfilled via coordination of an –OMe group (O7). The anionic part is the nitrate coordinated lanthanum complex where six nitrate ions are coordinated to a single La atom. The nearest distances between Co1…Co2, Co1…La1, and Co2…La1 were 7.215 (11), 7.335 (10), and 9.497 (11) Å, respectively. The plausible coordination modes of complexes **1** and **2** are shown in **Figure 1C**.

Bond valence sum (BVS) calculations were carried out to determine the oxidation states of the metal atoms in complexes 1 and 2, and the results are summarized in **Table 3** (Ghosh et al.,

TABLE 1 | Phase data of complexes 1 and 2.

Parameter	Complex 1	Complex 2
Formula	$C_{26}H_{34}Co_2N_2O_{12}$	$C_{47}H_{58}Co_2LaN_{17}O_{33}$
Formula weight (g mol^{-1})	684.41 g/mol	1,645.87 g/mol
Temperature (K)	101 K	100 K
Wavelength	0.71073 Å	0.71073 Å
Crystal system	Monoclinic	Monoclinic
Space group	$P2_1/c$ (14)	$P2_1/n$ (14)
Unit cell dimensions a, b, c (Å)	$a = 8.9157$ (14) Å, $b = 13.359$ (2) Å, $c = 24.066$ (4) Å	$a = 12.8836$ (11) Å, $b = 19.6476$ (17) Å, $c = 25.664$ (2) Å
α, β, γ (°)	$\alpha = 90, \beta = \beta = 90.602(6)°, \gamma = 90$	$\alpha = 90, \beta = 94.574(3)°, \gamma = 90$
V (Å^3)	2,866.22 (80) Å^3	6,475.69 (90) Å^3
Z	4	4
Density (g/cm^3)	1.58595 g/cm^3	1.68808 g/cm^3
Radiation type	Mo Kα	Mo Kα
μ (mm^{-1})	1.192	1.260
Absorption correction	Multiscan absorption correction	Multiscan absorption correction
Tmin, Tmax	0.867,0.898	0.970, 0.975
Rint	0.0835	0.1448
Theta (max) Ă$^{-3}$)	71.360	27.115
Refinement $R[F^2 > 2\sigma(F^2)]$, $wR(F^2)$, S	0.1239 (4,271), 0.3538 (4,562), 1.260	0.0565 (9,755), 0.1762 (14,277), 0.888
No. of reflections	4,562	14,277
No. of parameters	388	912
Data completeness	0.902	0.997

$R1 = \Sigma(||Fo| - |Fc||) / \Sigma |Fo|$.
$wR2 = [\Sigma[w(Fo^2 - Fc^2)^2] / \Sigma w[(Fo^2)^2]]^{1/2}$.
$S = [\Sigma[w(Fo^2 - Fc^2)^2] / (n-p)]^{1/2}$.
$w = 1/[\Sigma^2(Fo^2) + (m * p)^2 + n * p]$, $p = [max(Fo^2,0) + 2 * Fc^2]/3$, m and n are constants.

2019a). The calculated BVS data indicate that the two Co atoms in complex **1** are in +2 and +4 oxidations state, whereas in complex **2**, both the Co atoms are in +4 oxidation state, and the one La is in +3 oxidation state.

In the molecular geometry of complexes **1** and **2**, it is observed that in complex **1**, out of the two cobalt centers, the *o*-VED coordinated Co center is in +4 oxidation state, and the other cobalt center is in +2 oxidation state. Similarly, in complex **2**, both the Co centers are in +4 oxidation state and coordinated to two separate *o*-VED ligands. Thus, in these two complexes, it implies that the cobalt center coordinated to *o*-VED ligand is in +4 oxidation state otherwise, which is relatively unstable compared to Co in +2 and +3 oxidation state. So, here the *o*-VEDH₂ ligand may be playing an important role in stabilizing the +4 oxidation state of cobalt.

Moreover, these complexes were stabilized through intramolecular and intermolecular H-bonding (**Figure 2**) and van der Waals interactions (**Figures 3A,B**), and the corresponding bond lengths are shown in **Table 4** and ESI **Supplementary Table 1**, respectively.

Interestingly, complexes **1** and **2** have MOF structures those are constructed through catenation of 2D layers as shown in **Figure 4**. Among the two complexes, complex **1** has an excellent

MOF channel with size side of 2.44×6.221 Å along with diagonal side of 5.88×7.601 Å as shown in ESI **Supplementary Figure 1**.

Fourier Transform Infrared Spectroscopy (FTIR) Analysis

The FTIR spectra of complexes **1** and **2** are displayed in **Figure 5**, which shows the major peaks, wavenumber, and the interpretation of the possible functional groups. Selected IR data for complex **1** in cm^{-1}: 488 (b) for Co-N, 544 (m) for Co-O, 1,082 (m) For C-O, 1,225 (s) for C-N, 1,555 (m) for C=N, 1,638 (m) for C=C, and 3,260 (b) for C-H.

Selected IR data for complex **2** in cm^{-1}: 485 (b) for Co-N, 501 (b) for La-O, 545 (b) for Co-O, 1,082 (m) For C-O, 1,246 (s) for C-N, 1,607 (b) for C=N, 1,634 (m) for C=C, and 3,268 (b) for C-H.

Magnetic Study
DC Magnetic Study

The DC magnetic susceptibility of complexes (restrained in eicosane to prevent torqueing) was investigated under 3–300 K temperature and 0.1 T applied field. **Figure 6** shows the plot of $\chi_M T$ vs. T for complexes **1** and **2**. The observed room temperature value of $\chi_M T$ for compound **1** is 53.7 cm^3 mol^{-1} K. This value is the sum of contributions from both the Co^{II} and Co^{IV} in an uncoupled regime. We can calculate the expected contribution to the room temperature momentum from the Co^{II} ion (13.1 cm^3 mol^{-1} K) using the following value Co^{II} ($^4F_{9/2}$, $S = 3/2$, $L = 0$, $g = 2$). However, the calculation of the contribution from the Co^{IV} ion is not as straightforward. The $\chi_M T$ value appears to be higher than those expected in the spin-only case: Co^{IV} ($^6S_{5/2}$, $S = 5/2$, $L = 0$, $g = 2$). Upon cooling down to 19 K, it steadily decreases to a value of 40.6 cm^3 mol^{-1} K and down to 2 K, after it increases dramatically up to 56.1 cm^3 mol^{-1} K, which suggests either ferromagnetic interaction or ferromagnetic behavior.

The $\chi_M T$ value in room temperature of complex **2** is −0.03 cm^3 mol^{-1} K, which is very low than expected value of non-interacting two Co^{IV} ions ($^6S_{5/2}$, $S = 5/2$, $L = 0$, $g = 2$) and one La^{III} ($^1S_0$, $S = 0$, $L = 0$, $g = 1$). The $\chi_M T$ for complex **2** remains constant at a value of approximately −0.03 cm^3 mol^{-1} K at 300 K, down to 55 K; it steadily increases to a value 0.47 cm^3 mol^{-1} K and down to 2 K at 0.34 cm^3 mol^{-1} K with dramatic decrease, which suggests either antiferromagnetic interaction or antiferromagnetic behavior. Total spin (*S*) and corresponding exchange coupling constant (*J*) values for complexes **1** and **2** are 4 and 5 and 0.260 cm^{-1} and 0.043 cm^{-1} respectively.

AC Magnetic Study

AC susceptibility (in phase and out phase) studies have been conducted for the complexes in between 1.8 and 15 K in a zero applied field with 3.5 Oe driving field to investigate for slow magnetic relaxation, i.e., SMM behavior. The AC susceptibility studies for complexes **1** and **2** have been performed at various frequencies such as 50, 250, and 550 H, and a plot of $\chi_M T$ vs. temperature is presented in **Figures 7**, **8**, respectively.

The alternating current (ac) in-phase susceptibility of complexes **1** and **2** is in good agreement with the direct current

TABLE 2 | Selected bond distances (Å) and bond angles (°) for complexes 1 and 2.

Bond length					
Complex 1		Complex 2			
Bond type	Bond length (Å)	Bond type	Bond length (Å)	Bond type	Bond length (Å)
Co1-N2	1.856 (8)	La1-O24	2.585 (4)	Co1-N1	1.878 (5)
Co1-N1	1.876 (8)	La1-O14	2.604 (4)	Co1-N2	1.889 (4)
Co1-O8	1.892 (7)	La1-O29	2.613 (4)	Co1-O2	1.901 (4)
Co1-O2	1.895 (7)	La1-O27	2.625 (4)	Co1-O1	1.916 (4)
Co1-O1	1.902 (7)	La1-O23	2.651 (4)	Co1-N3	1.941(4)
Co1-O4	1.920 (7)	La1-O26	2.651 (4)	Co1-N4	1.944 (5)
Co2-O10	2.004 (8)	La1-O21	2.652 (4)	Co2-N7	1.876 (4)
Co2-O7	2.065 (8)	La1-O18	2.654 (4)	Co2-N6	1.884 (4)
Co2-O5	2.14 (8)	La1-O20	2.659 (4)	Co2-O6	1.911 (4)
Co2-O3	2.062 (8)	La1-O30	2.662 (4)	Co2-O5	1.914 (4)
Co2-O1	2.069 (7)	La1-O17	2.663 (4)	Co2-N8	1.950 (4)
Co2-O2	2.137 (7)	La1-O15	2.749 (4)	Co2-O7	1.973 (4)

Bond angle					
Bond type	Angle (°)	Bond type	Angle (°)	Bond type	Angle (°)
N2-Co1-N1	86.0 (4)	N1-Co1-N2	84.7 (2)	O24-La1-O14	175.53 (14)
N2-Co1-O8	95.7 (3)	N1-Co1-O2	93.56 (18)	O24-La1-O29	65.99 (13)
N1-Co1-O8	92.5 (3)	N2-Co1-O2	178.11 (18)	O14-La1-O29	110.64 (13)
N2-Co1-O2	95.5 (3)	N1-Co1-O1	177.3 (2)	O24-La1-O27	68.90(14)
N1-Co1-O2	178.4 (3)	N1-Co1-N2	84.7 (2)	O14-La1-O27	107.52 (12)
O8-Co1-O2	87.8 (3)	N1-Co1-O2	93.56 (18)	O29-La1-O27	71.89 (14)
N2-Co1-O1	178.0 (3)	N2-Co1-O2	178.11 (18)	O24-La1-O23	48.55 (14)
N1-Co1-O1	94.0 (3)	N1-Co1-O1	177.3 (2)	O14-La1-O23	133.13 (14)
O8-Co1-O1	86.4(3)	N1-Co1-N2	84.7 (2)	O29-La1-O23	110.73 (14)
O2-Co1-O1	84.4 (3)	N1-Co1-O2	93.56 (18)	O27-La1-O23	66.46 (13)
N2-Co1-O4	87.7 (3)	N2-Co1-O2	178.11 (18)	O24-La1-O26	110.94 (14)
N1-Co1-O4	88.1 (3)	N1-Co1-O1	177.3 (2)	O14-La1-O26	64.72 (12)
O8-Co1-O4	176.6 (3)	N1-Co1-N2	84.7 (2)	O29-La1-O26	70.08 (13)
O2-Co1-O4	91.4 (3)	N1-Co1-O2	93.56 (18)	O27-La1-O26	47.96 (12)
O1-Co1-O4	90.3 (3)	N2-Co1-O2	178.11 (18)	O23-La1-O26	111.21 (13)
O10-Co2-O7	91.7 (3)	N7-Co2-N6	84.88 (19)	O24-La1-O21	71.91 (13)
O10-Co2-O3	88.4 (3)	N7-Co2-O6	177.20 (18)	O14-La1-O21	110.10 (12)
O7-Co2-O3	173.3 (3)	N6-Co2-O6	94.15 (17)	O29-La1-O21	70.17 (14)
O10-Co2-O1	156.9 (3)	N7-Co2-O5	93.15 (17)	O27-La1-O21	133.63 (14)
O7-Co2-O1	91.6 (3)	N6-Co2-O5	177.96 (17)	O23-La1-O21	103.85 (13)
O3-Co2-O1	85.8 (3)	O6-Co2-O5	87.79 (15)	O26-La1-O21	133.96 (13)
O10-Co2-O2	127.0 (3)	N7-Co2-N8	91.12 (18)	O24-La1-O18	117.68 (14)

TABLE 3 | Bond valence sums[b] for complexes 1 and 2[a].

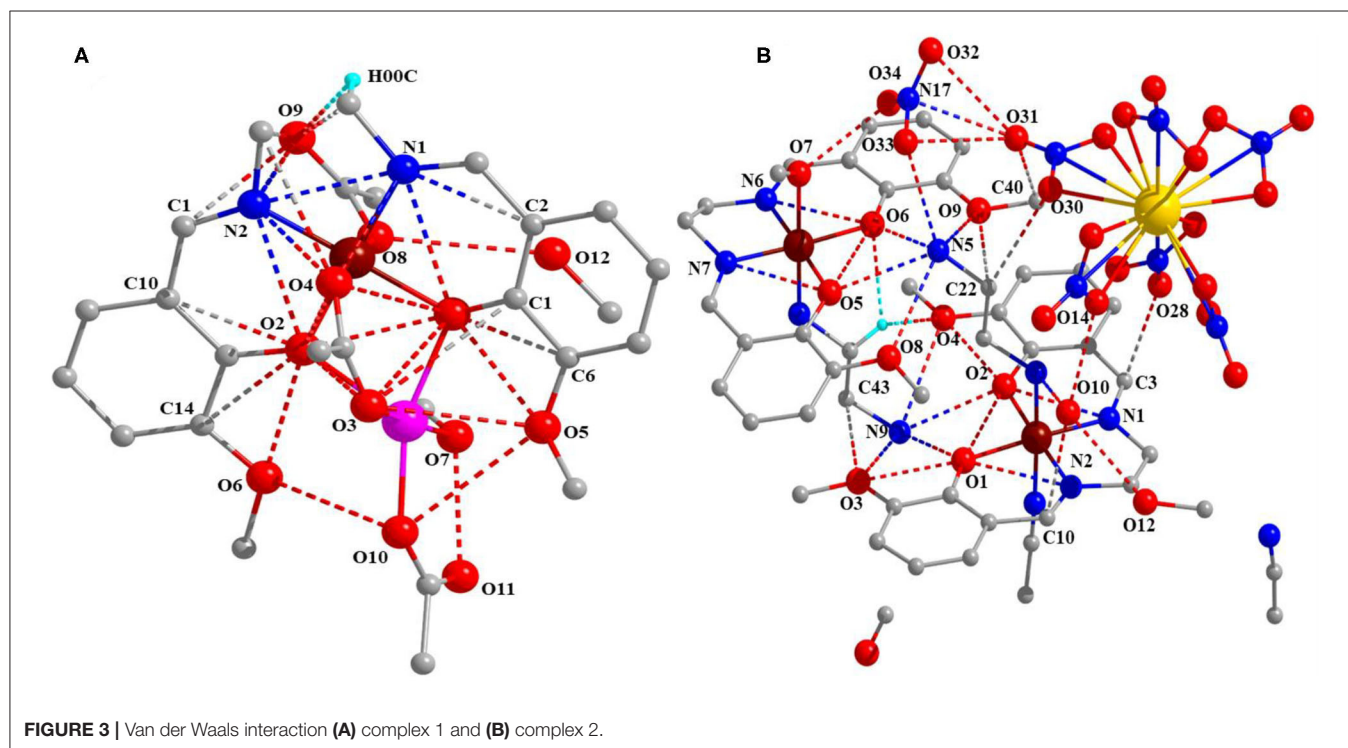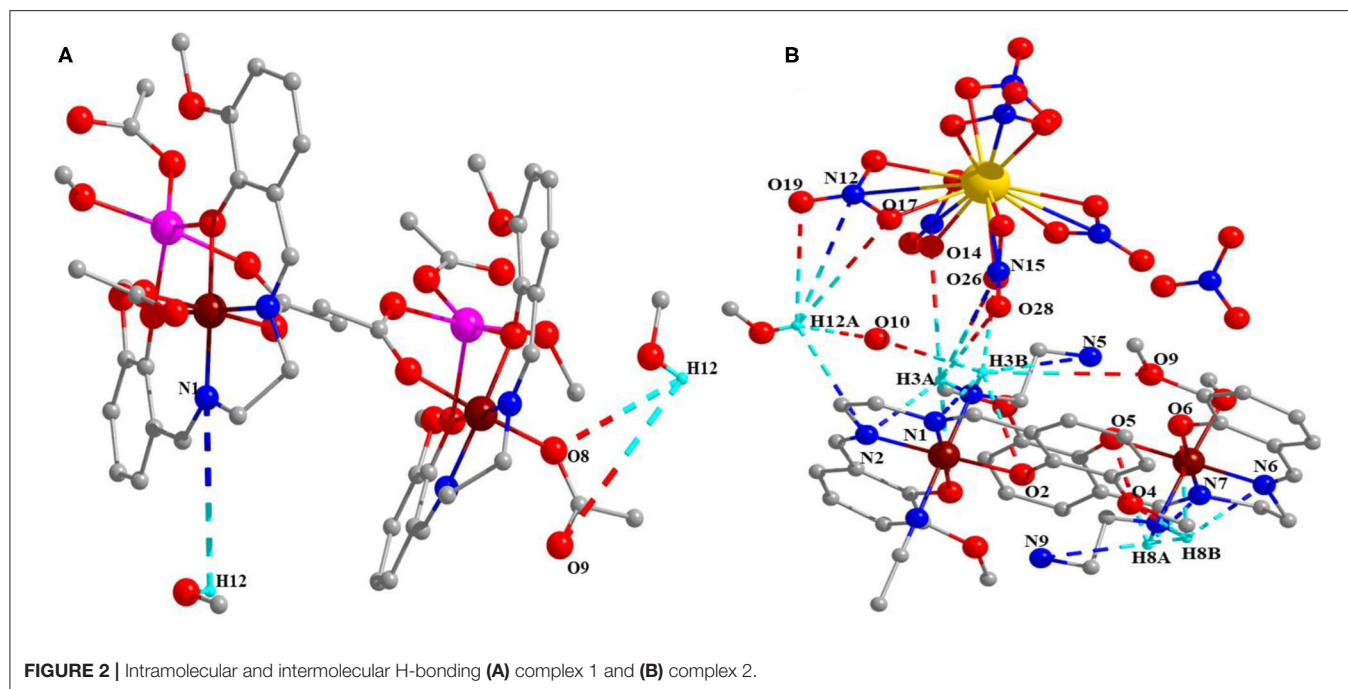| Complex 1		Complex 2		
Co₁ᴵⱽ	Co₂ᴵᴵ	Co₁ᴵⱽ	Co₂ᴵⱽ	Laᴵᴵᴵ
4.13	1.97	4.43	4.14	3.34

[a]The oxidation state of a particular atom is the nearest integer to the underlined value.
[b]The underlined value is the closest to the charge for which it was calculated.

(dc) data at the same temperature. In the case of complex **1**, $\chi_M T$ value is a sharp decrease from 2 to 5 K, and then it is dramatically increased from 5 to 8 K, reaching the maximum $\chi_M T$ value

of 0.025 cm³ Kmol⁻¹ (**Figure 7**) at about 7 K temperature. The frequency-dependent rise in the out-of-phase susceptibility is observed as a peak tail, indicating that **1** displays behavior characteristic of a SMM.

For complex **2**, $\chi_M' T$ value is significantly increased with increasing the temperature, having a maximum value of 1.104 cm³ Kmol⁻¹ at 10 K. Similarly, **1** continues to show a decrease in $\chi_M' T$ with increasing temperatures before a slight frequency-dependent drop is observed at low temperature. Also equal to **1**, a frequency-dependent rise in the out-of-phase susceptibility is observed as peak tail, indicating that **2** also displays behavior characteristic of a SMM.

FIGURE 2 | Intramolecular and intermolecular H-bonding **(A)** complex 1 and **(B)** complex 2.

FIGURE 3 | Van der Waals interaction **(A)** complex 1 and **(B)** complex 2.

Other Studies

Optical Properties

The optical band gap of the complexes has been computed from Tauc's equation (**1**) to explain the conductivity of isolated complexes:

$$(\alpha h\upsilon)^n = A(h\upsilon - E_g) \quad (1)$$

where α denotes the absorption coefficient, and it is calculated by $\alpha = (2.303 \times \text{absorption})/t$, $t = $ cubet thickness (1 cm), A refers to constant, E_g indicates the band gap energy, exponent n depends on the type of transition, and h denotes the Planck's constant.

Equation **1** was used to plot $(\alpha h\upsilon)^2$ vs. $h\upsilon$ (**Figure 9**) from which band gap energy (E_g) of the complexes was calculated by extrapolating the linear portion of the curve to

TABLE 4 | Selected H-bond length (Å) for complexes 1 and 2.

Complex 1		Complex 2	
Bond type	Bond length (Å)	Bond type	Bond length (Å)
O8 … H12	3.233	H12A … O17	3.867
H12 … O9	4.598	H12A … O19	3.392
N1 … H12	4.119	H3B … O26	2.501
		H3B … N5	3.942
		H3A … O25	3.999
		H3A … O26	3.202
		H3A … O28	3.9917

$(\alpha h\upsilon)^2 = 0$. The values of band gap energy of complexes **1** and **2** were 3.7 and 3.03 eV, respectively. These results are significant for solar, optoelectronic, and electronic applications because of a small band gap in energy, which extends the electronic progress from HOMO-LUMO to the increased electrical conductivity of the complexes (Brown and Altermatt, 1985; Sengupta et al., 1998; Turan et al., 2014; Ahmed et al., 2016). The band gap value suggests that complexes may act as semiconductor materials.

H$_2$O$_2$ Sensing

To determine the sensing capacity of the complexes we have used H$_2$O$_2$ as source materials. We have added 1 mL of 20 mM H$_2$O$_2$ to 3 mL solution of the complexes, and the electronic spectra were recorded at regular intervals. **Figure 10A** shows that the absorbance of complex **1** decreased with increasing the time in presence H$_2$O$_2$. After 10 min, we have observed that the characteristic peak of complex **1** at 274 nm was disappearing, and the color intensity of complex **1** turns from faded yellow to colorless. This is possible for the presence of Co(II), which should be oxidized to Co(III), and OH could be formed. During the decomposition reactions of H$_2$O$_2$ by complex **1**, hydroxyl radicals (OH) are probably formed and acted as an oxidant, which oxidizes Co(II) to Co(III)/Co(IV) and itself produces H$_2$O; as a result, the absorbance of the solution mixture was decreased as observed in the UV-visible spectra. But such kind of H$_2$O$_2$ decomposition was not observed in complex **2**, which may be because Co sites already exist in higher (+4) oxidation state, and they do not form radicals. Therefore, complex **2** does not show the H$_2$O$_2$ decomposition properties. The degradation of complex **1** was followed by first-order kinetic reaction, and the rate constant (k) was found to be 1.59×10^{-4} S^{-1} shown in **Figure 10B**.

DNA Binding

Before adding CT-DNA to the complexes, the stability of complex **1**, complex **2**, and o-VEDH$_2$ in Tris-HCl buffer solution was measured by UV-visible spectroscopy at room temperature for 1 h (each in 150-min interval), and the absorption peaks were not changed. The UV-visible absorption spectra of complexes **1** and **2** are represented in **Figures 11A,B**, respectively. The absorption peaks at 384 nm of complex **1** and at 291 and 361 nm of complex

2 are assigned for the d–d transition. To study the binding characteristics of complexes **1** and **2** with CT-DNA, CT-DNA was stepwise added to the solution of the complexes in a cuvette separately, and absorption spectra were recorded in each step. In case of complex **1**, except slight decrease in absorption, no characteristic change was observed. However, in case of complex **2** upon stepwise addition of 20, 40, 60, and 80 μL of CT-DNA, the characteristic absorption at 291 gradually shifts to 289, 288, 286, and 285 nm (blue shift), whereas the characteristic peak at 361 nm gradually changes to 360, 359, and 358 nm (blue shift), respectively. This change in absorption characteristics indicates some short of interaction between complex **2** and CT-DNA; however, the nature of this interaction is yet to be established. Complex 2 contains nitrate, which could form H-bond with CT-DNA shown in ESI S2, whereas for complex **1**, the capability to form H-bond with CT-DNA is probably lower because all O, N, and H atoms of complex 1 should be busy in formation of intramolecular H-bonding.

The absorption spectra of the complex binding to DNA may be through intercalation, revealing that blue shift appears because of strong staking interaction between complex **2** and base pairs of DNA. The binding constant K_b of complex **2** was determined by the equation (Fu et al., 2005) as follows:

$$[\mathbf{DNA}] \times (\boldsymbol{\varepsilon_a} - \boldsymbol{\varepsilon_f})^{-1} = [\mathbf{DNA}] \times (\boldsymbol{\varepsilon_b} - \boldsymbol{\varepsilon_f})^{-1} + \mathbf{K_b}^{-1}$$
$$\times (\boldsymbol{\varepsilon_b} - \boldsymbol{\varepsilon_f})^{-1}$$

where $\boldsymbol{\varepsilon_a}$, $\boldsymbol{\varepsilon_f}$, and $\boldsymbol{\varepsilon_b}$ were denoted as extinction coefficient of the complex, CT-DNA, and bound complex, respectively. The binding constant of complex **2** was 1.22×10^5 M^{-1} shown in **Table 5**. Therefore, binding constant values lie within the range of a characteristic of the CT-DNA binding by complexes through intercalative mode (Wolfe and Shimer, 1987; Patel et al., 2011).

CONCLUSION

In the present work, we have successfully synthesized two novel Co^{II}Co^{IV} and Co$_2^{IV}$La^{III} complexes utilizing o-VEDH$_2$ as Schiff base ligand from two different reaction conditions and investigated their SMMs properties, as well as multifunction activities, such as H$_2$O$_2$ sensors and DNA binders. In solid state, both the complexes show the formation of MOFs structures. Complexes **1** and **2** have optical band gap energy of 3.7 and 3.03 eV, which indicates that these may have semiconductor properties. Interestingly, it is also established that complex **1** has H$_2$O$_2$-sensing properties with a rate constant (k) = 1.59×10^{-4} s^{-1}, whereas complex **2** is bound to CT-DNA by intercalation binding mode with binding constant $k_b = 1.22 \times 10^5$ M^{-1}.

EXPERIMENTAL

Materials and Methods

All the reagent-grade chemicals were purchased from Sigma–Aldrich, India, and were used as received without further purification. All the reaction solvents were also used as received.
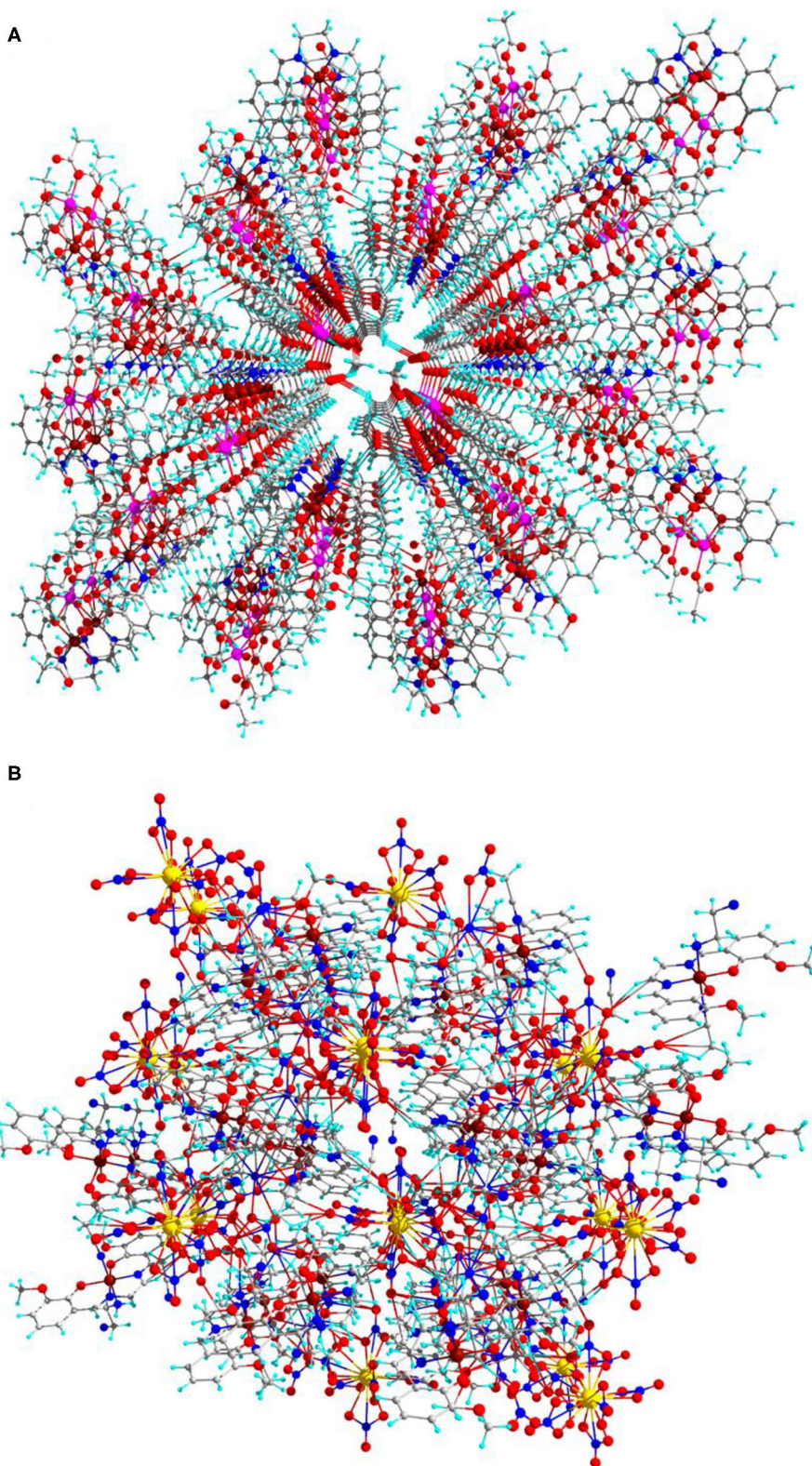
FIGURE 4 | Catenation 2D layers MOF **(A)** for complex 1 and **(B)** for complex 2 (central projection, along 100-a axis) in ball-and-stick model.
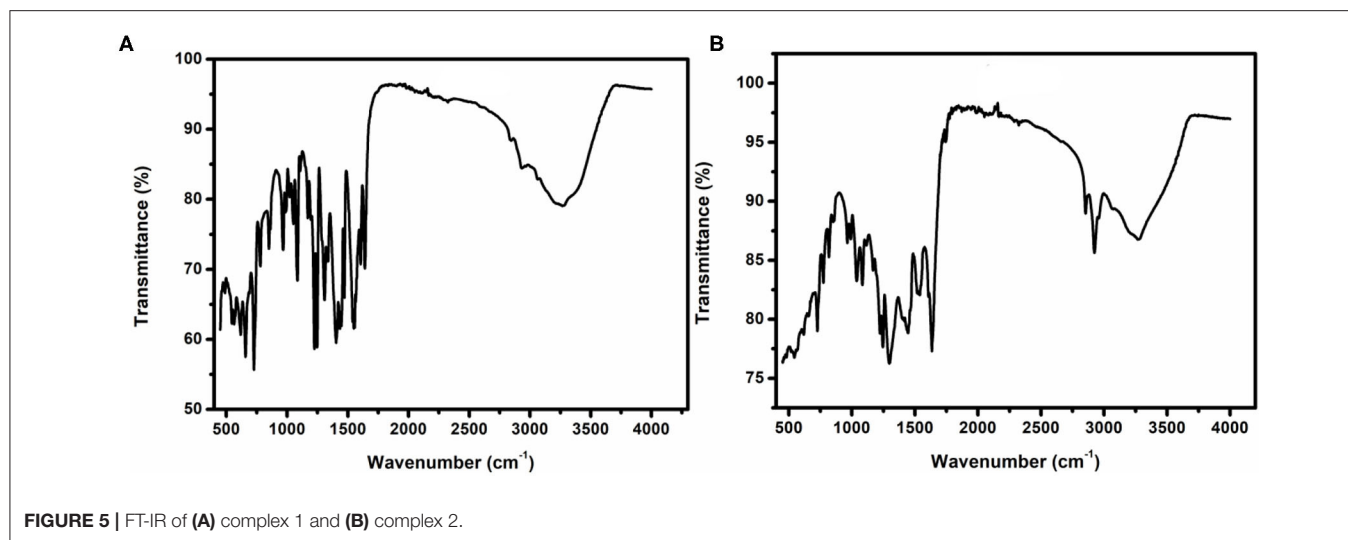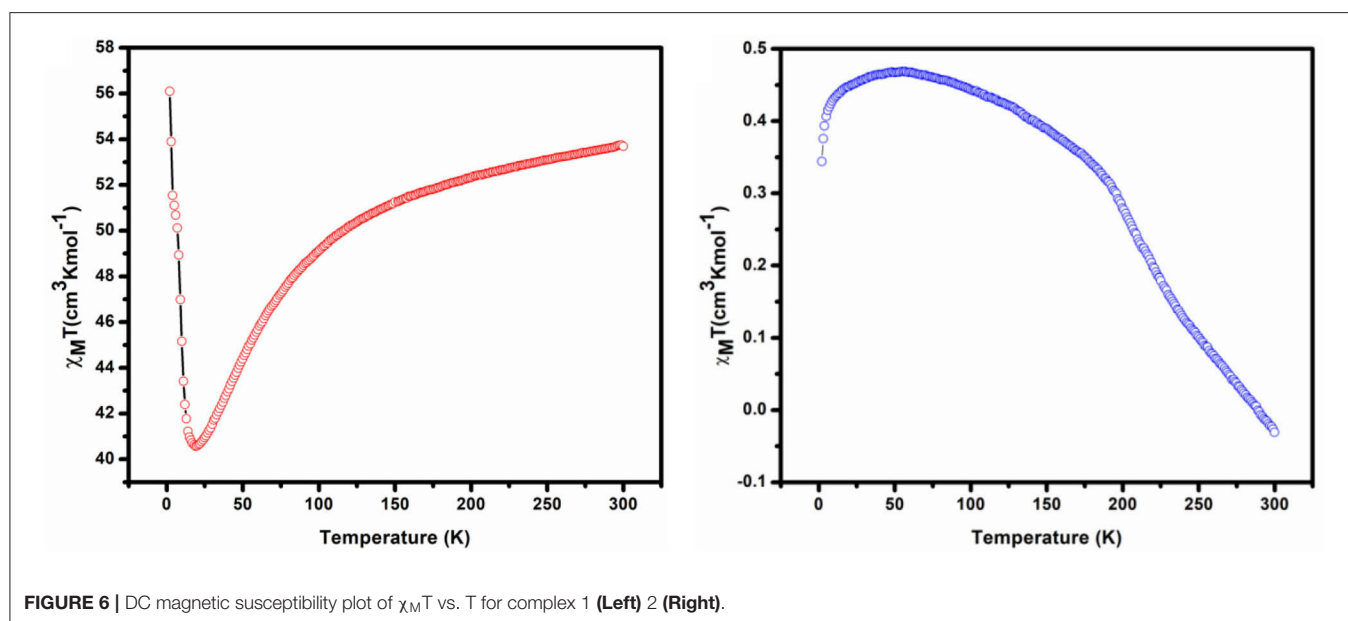
FIGURE 5 | FT-IR of **(A)** complex 1 and **(B)** complex 2.

FIGURE 6 | DC magnetic susceptibility plot of χ_MT vs. T for complex 1 **(Left)** 2 **(Right)**.

Syntheses

Schiff Base Ligand

The Schiff base ligand N,N′-bis(o-vanillinidene) ethylenediamine (o-VEDH$_2$) was synthesized in the following procedure (**Scheme 1**) and also reported in our earlier publication (Ghosh et al., 2019b):

$$[Co^{II}Co^{IV}(o - VED)(OAc)_2(\cdot\mu_2 - OAc)(OMe)]\bullet MeOH \quad (1)$$
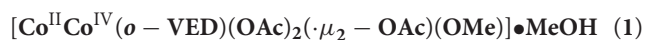
Co(acac)$_2$ (0.487g, 3 mmol) was dissolved in 10 mL methanol followed by dropwise addition of o-VEDH$_2$ (0.305g, 1 mmol) (separate solution in MeCN) and stirred for more than 2 h until a clear solution was obtained. Finally, the resulting solution was filtered and divided into two parts. One part of the black color filtrate was kept for slow evaporation, and another part was layered over diethyl ether. In a week, black single crystals were

obtained in both the conditions in high yield. The single crystals were separated out from the mother solution and were washed with diethyl ether (two to three times). The analytically pure compound was obtained after drying under vacuum.

Yield: 33% (60 mg). Anal. Calcd. for **C$_{26}$ H$_{34}$Co$_2$N$_2$O$_{12}$ (1)**: C, 28.32; H, 5.12; N, 3.94%. Found: C, 27.91; H, 4.89; N, 3.88%. Selected IR data in cm^{-1}: 488 (b), 544 (m), 1,082 (m), 1225 (s), 1,555 (m), 1,638 (m), and 3,260 (b) (s = strong, m = medium, b = broad). Detailed discussion of IR spectrum of **1** is provided in **Figure 5A**.

$$[Co_2^{IV}(o - VED)_2(en)_2(NCCH_3)(OCH_3)]$$
$$[La(NO_3)_6](NO_3^-)\bullet 2MeOH\bullet MeCN\bullet H_2O \quad (2)$$
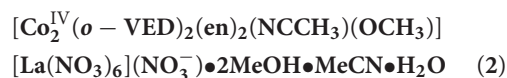
Solution of La(NO$_3$)$_3$·6H$_2$O (0.054g, 1 mmol) in MeOH (10 mL) was added dropwise to a stirred solution of o-VEDH$_2$ (0.081g, 2
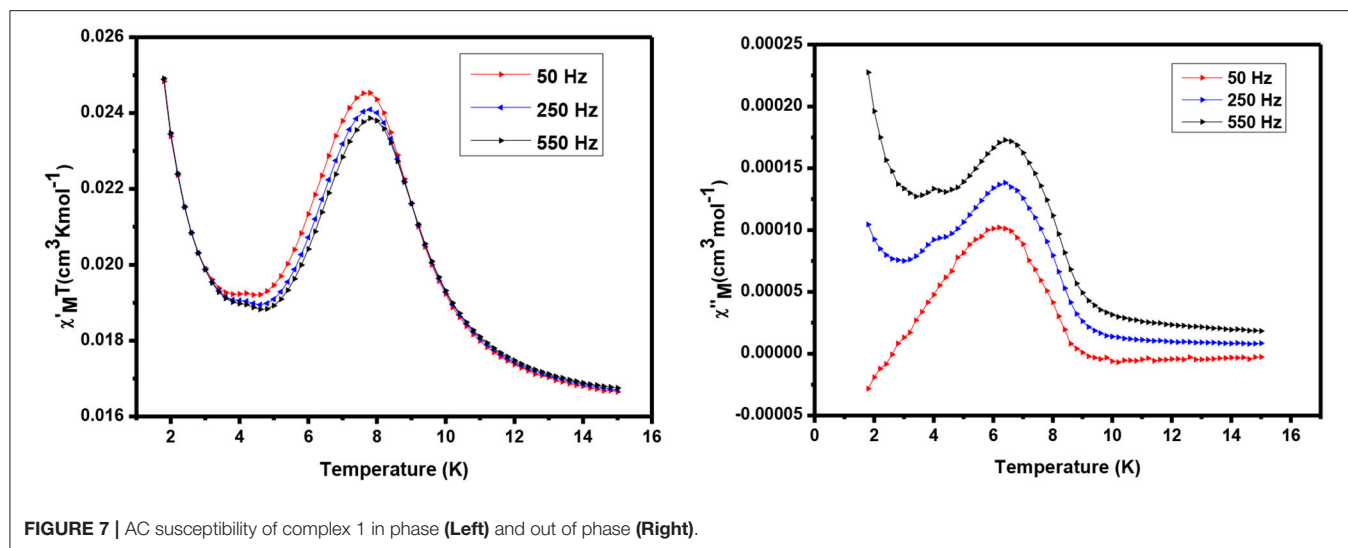
FIGURE 7 | AC susceptibility of complex 1 in phase **(Left)** and out of phase **(Right)**.
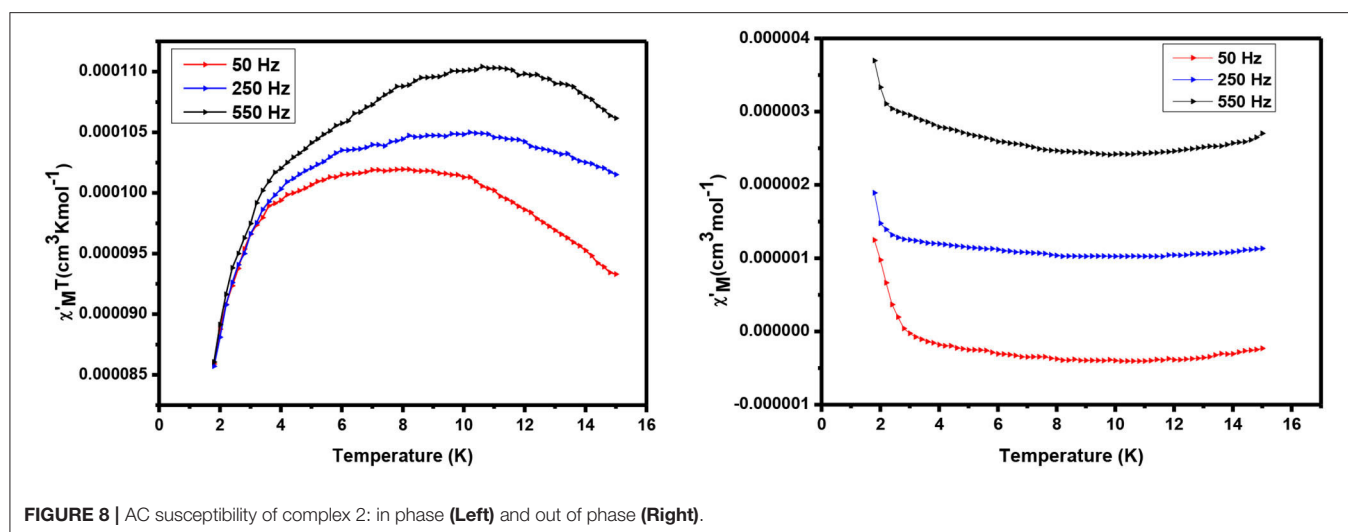

FIGURE 8 | AC susceptibility of complex 2: in phase **(Left)** and out of phase **(Right)**.

mmol) in MeCN (10 mL). The reaction mixture was kept stirring, and solid Co(NO$_3$)$_2$·6H$_2$O (0.037g, 1 mmol) was added after 15 min. Further, solid iodine (0.063 g, 2 mmol) was added to the reaction mixture and was vigorously stirred for additional 2 h to obtain a black color solution. The black color solution was filtered, and the filtrate was divided into two parts. One part of the filtrate was kept for slow evaporation, and the other part was layered over CH$_3$Cl. In a week, high-quality black single crystals were obtained from the CH$_3$Cl layered solution in high yield. The crystals were separated out and were washed with diethyl ether (two to three times) before drying under vacuum.

Yield: 20% (1.2 mg). Anal. Calcd. for **C$_{47}$H$_{58}$Co$_2$LaN$_{17}$O$_{33}$ (2)**: C, 28.32; H, 3.55; N, 14.37%. Found: C, 28.34; H, 3.52; N, 14.29%. Selected IR data in cm^{-1}: 485 (b), 501 (b), 545 (b), 1,082 (m), 1,246 (s), 1,607 (b), 1,634 (m), and 3,268 (b) [s = strong, m = medium, b = broad]. Detailed discussion of IR spectrum of **2** is provided in **Figure 5B**.

Physical Measurements

The ^{1}H NMR spectra of Schiff base ligand were recorded in a JEOL 400-MHz spectrophotometer. Infrared spectra were recorded in a PerkinElmer FTIR spectrometer in the solid state (KBr pellets) in the 400- to 4,000-cm^{-1} range. Elemental analyses (C, H, and N) and X-ray crystallography were performed through central facilities at IACS, Kolkata. Shimadzu UV-1800 spectrophotometer was used to record the electronic spectrum of complexes. Quantum Design MPMS-XL SQUID magnetometer (IISER Bhopal) equipped with a 7-T magnet and operating in the 1.8- to 300-K range was used on vacuum dried solids to collect variable-temperature dc and ac magnetic susceptibility data. Samples were embedded in solid eicosane in a gel capsule to prevent torqueing. Diamagnetic and background contributions from the eicosane and gel capsule were measured as a blank and subtracted from the susceptibility. Magnetization vs. field and temperature data was fit using the program MAGNET (Davidson, 1999). Pascal's
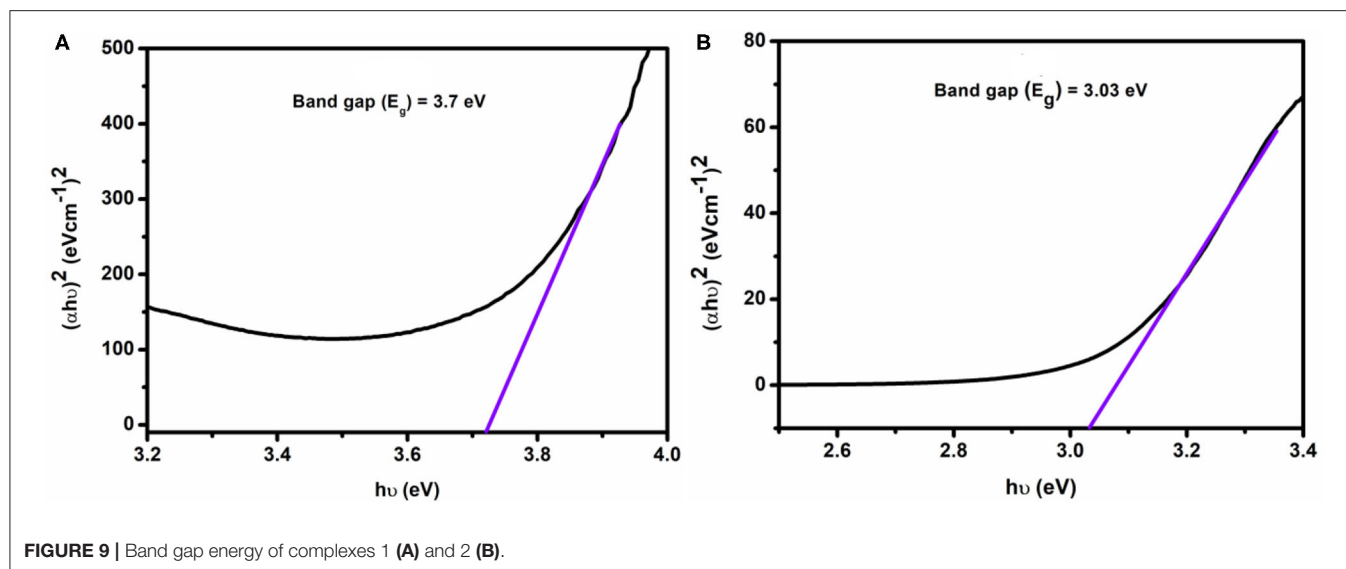
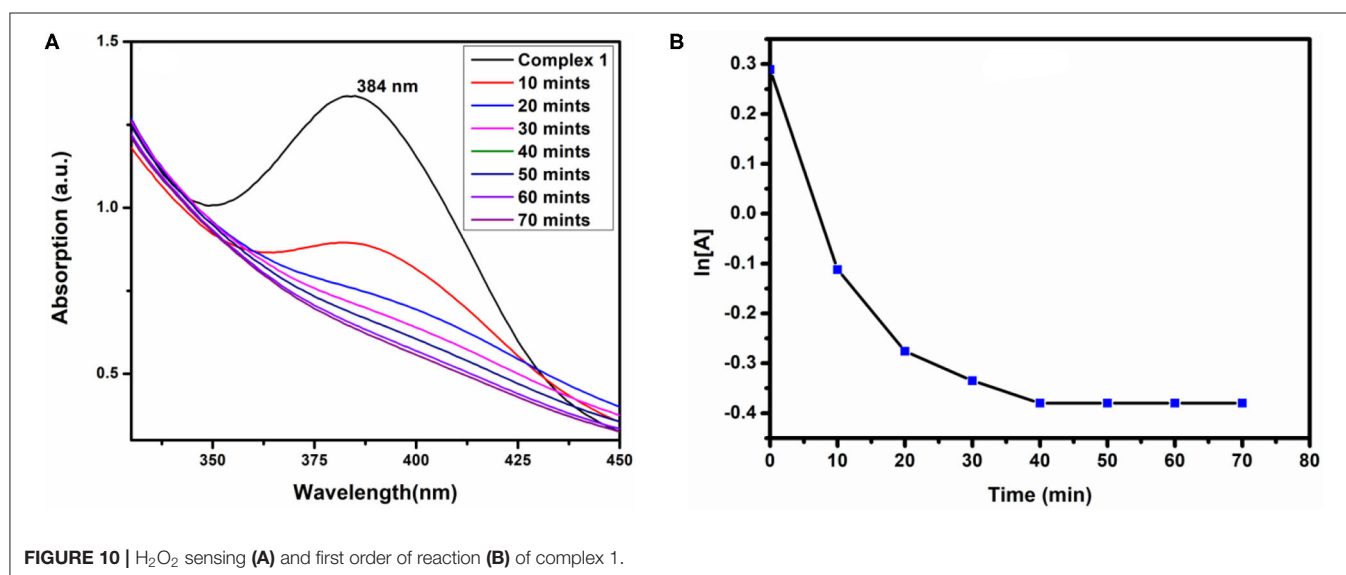**FIGURE 9 |** Band gap energy of complexes 1 **(A)** and 2 **(B)**.

FIGURE 10 | H$_2$O$_2$ sensing **(A)** and first order of reaction **(B)** of complex 1.

constants (Weast and Astle, 1984) were used to estimate the diamagnetic correction, which was subtracted from the experimental susceptibility to give the molar paramagnetic susceptibility (χ_M).

Crystallographic Data Collection and Refinement

On the Bruker SMART APEX CCD diffractometer with SMART/SANTI programming, a single-precious-stone X-beam data were collected for complexes **1** and **2** at 293 K/100 K (Sheldrick, 2008). MoKα graphite monochromatized (0.71073 Å) radiation was used for the collection of intensity information at 100 K. A coordinated strategy using SHELXS-2013, which was incorporated into WinGX, understood the structures (Farrugia, 2012, 2013; Sheldrick, 2013) SADABS was associated with exact corrections to the absorption (Sheldrick, 1996).

An anisotropic displacement coefficient was used to refine all non-hydrogen particles. The particles of hydrogen carbon were integrated into geometric positions and given warm parameters 1, 2 those of the molecule to which they were attached. An initial search for reciprocal space exposed that both complexes are crystallized in monoclinic phase with P21/c and P21/nspace group.

The consequences of the precious crystal data and structure refined information of complexes **1** and **2** are available in **Table 1**, respectively.

Hydrogen Peroxide Sensing Capacity of the Complexes

The H$_2$O$_2$ detection protocol is already discussed in our previous article (Bera and Raj, 2013; Ghosh et al., 2019b). Initially, complexes were dissolved in CH$_3$CN to obtain a
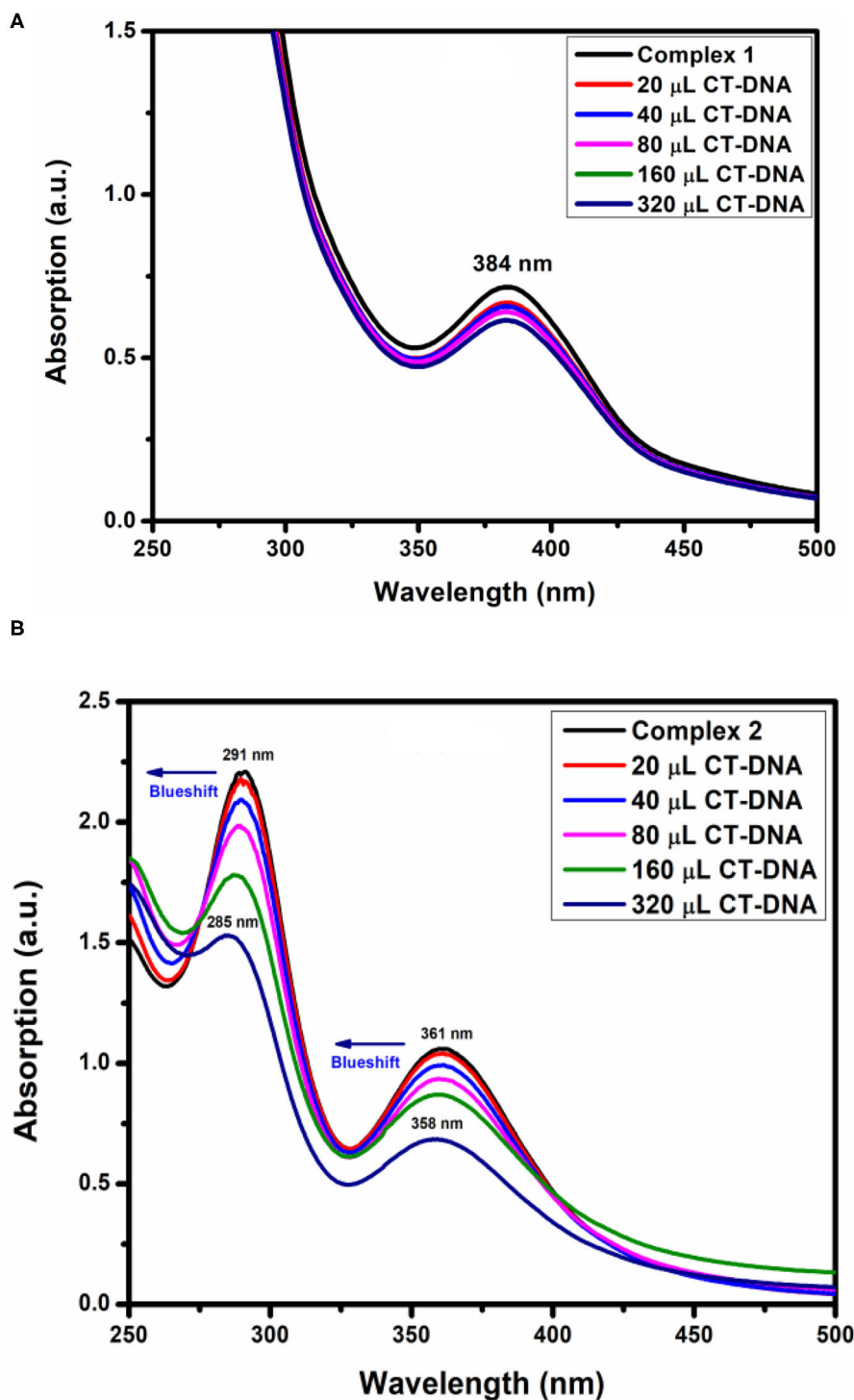
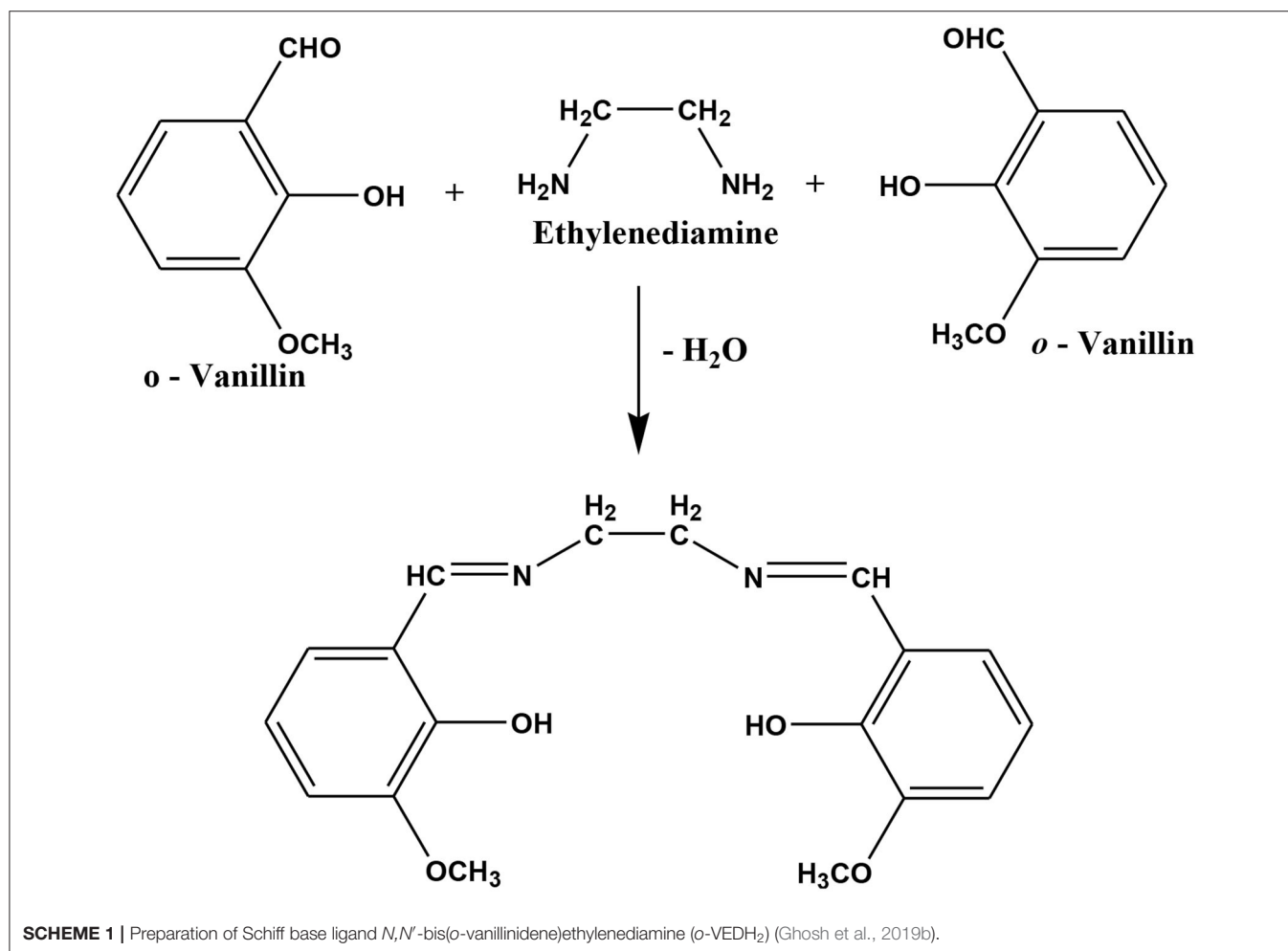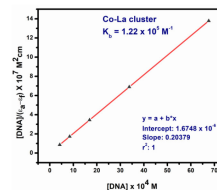**FIGURE 11 |** DNA-binding study **(A)** complex 1 and **(B)** complex 2.

suitable dilute solution for the initial of UV-visible spectrum. In 3 mL of the above solution, 1 mL 20 mM H$_2$O$_2$ was added. Spectra were recorded at regular intervals in a UV-visible spectrophotometer.

DNA-Binding Study

CT-DNA was dissolved in Tris-HCl buffer (pH 7.25) solution. and its purity was confirmed from the obtained absorbance ratio of A260/A280 in the range of 1.8 to 1.9.

TABLE 5 | Absorption titration data of complexes **1** and **2**.

Complex 2			
Absorption	[DNA]/($\varepsilon_a - \varepsilon_f$) × 10^7 M^2 cm	[DNA] ×10^4 M	K_b (M^{-1})
1.063	0.000	0.000	1.217 × 10^5 M^{-1}
1.038	0.861	4.226	
0.988	1.722	8.451	
0.937	3.446	16.909	
0.870	6.889	33.806	
0.686	13.779	67.611	

SCHEME 1 | Preparation of Schiff base ligand *N,N′*-bis(*o*-vanillinidene)ethylenediamine (*o*-VEDH$_2$) (Ghosh et al., 2019b).

Metal complexes **1** and **2** were dissolved, and absorption titration experiments were performed using the increased concentration of CT-DNA with the constant amount of the metal complex.

DATA AVAILABILITY STATEMENT

The datasets presented in this study can be found in online repositories. The names of the repository/repositories and accession number(s) can be found in the article/**Supplementary Material**.

AUTHOR CONTRIBUTIONS

Synthesis and applications were performed by MKG. The crystallography of the complexes was performed by BJ. The manuscript was designed and written by MKG and TKG. All the authors have given approval to the final version of the manuscript.

FUNDING

No. A/R&D/RP-2/ Phy&Engg./2017-18/271) and Indira Gandhi National Tribal University, Amarkantak, Madhya Pradesh.

SUPPLEMENTARY MATERIAL

The Supplementary Material for this article can be found online at: https://www.frontiersin.org/articles/10.3389/fchem.2020.571223/full#supplementary-material

REFERENCES

Ahmed, A. H., Hassan, A. M., Gumaa, H. A., Mohamed, B. H., Eraky, A. M., and Omran, A. A. (2016). Copper (II)-oxaloyldihydrazone complexes: physico-chemical studies: energy band gap and inhibition evaluation of free oxaloyldihydrazones toward the corrosion of copper metal in acidic medium. *Arab. J. Chem.* 12, 4287–4302. doi: 10.1016/j.arabjc.2016.05.015

Alghool, S., El-Halim, H. F. A., El-Sadek, M. A., Yahia, I. S., and Wahab, L. A. (2013). Synthesis, thermal characterization, antimicrobial activity of lanthanum, cerium, thorium complexes of amino acid Schiff base ligand. *J. Ther. Anal. Calorimetry* 112, 671–681. doi: 10.1007/s10973-012-2628-4

Bera, R. K., and Raj, C. R. (2013). A facile photochemical route for the synthesis of triangular Ag nanoplates and colorimetric sensing of H$_2$O$_2$. *J. Photochem. Photobiol A: Chem.* 270, 1–6. doi: 10.1016/j.jphotochem.2013.07.005

Bogani, L., and Wernsdorfer, W. (2010). "Molecular spintronics using single-molecule magnets," in *Nanoscience and Technology: A Collection of Reviews from Nature Journals* (World Scientific), 194–201. doi: 10.1142/9789814287005_0020

Brown, I. D., and Altermatt, D. (1985). Bond-valence parameters obtained from a systematic analysis of the inorganic crystal structure database. *Acta.Crystallogr. Sect. B* 41, 244–247. doi: 10.1107/S0108768185002063

Chelebaeva, E., Larionova, J., Guari, Y., Ferreira, R. A., Carlos, L. D., Paz, F. A. A., et al. (2009). Luminescent and magnetic cyano-bridged coordination polymers containing 4d– 4f ions: toward multifunctional materials. *Inorg. Chem.* 48, 5983–5995. doi: 10.1021/ic900378d

Clough, A. J., Skelton, J. M., Downes, C. A., de la Rosa, A. A., Yoo, J. W., Aron, W., et al. (2017). Metallic conductivity in a two-dimensional cobalt dithiolene metal–organic framework. *J. Am. Chem. Soc.* 139, 10863–10867. doi: 10.1021/jacs.7b05742

Davidson, E. R. (1999). Indiana University: Bloomington, IN.

Ding, Y. S., Chilton, N. F., Winpenny, R. E., and Zheng, Y. Z. (2016). On approaching the limit of molecular magnetic anisotropy: a near-perfect pentagonal bipyramidal dysprosium (III) single-molecule magnet. *Angew. Chem. Int. Ed.* 55, 16071–16074. doi: 10.1002/anie.201609685

Dong, Z., Sun, Y., Chu, J., Zhang, X., and Deng, H. (2017). Multivariate metal–organic frameworks for dialing-in the binding and programming the release of drug molecules. *J. Am. Chem. Soc.* 139, 14209–14216. doi: 10.1021/jacs.7b07392

Droge, W. (2002). Free radicals in the physiological control of cell function. *Physiol. Rev.* 82, 47–95. doi: 10.1152/physrev.00018.2001

Farrugia, L. J. (2012). WinGX and ORTEP for Windows: an update. *J. Appl. Crystallogra.* 45, 849–854. doi: 10.1107/S0021889812029111

Farrugia, L. J. (2013). *WinGX, version 3 2013*, Department of Chemistry, University of Glasgow.

Freitas, A. R., Rubira, A. F., and Muniz, E. C. (2010). Polychloroprene degradation by photo-fenton. Conductivity measures as new approach for detecting/evaluation of degradation products. *J. Polym. Environ.* 18, 668–673. doi: 10.1007/s10924-010-0226-8

Fu, M. L., Guo, G. C., Liu, X., Liu, B., Cai, L. Z., and Huang, J. S. (2005). Syntheses, structures and properties of three selenoarsenatestemplated by transition metal complexes. *Inorg. Chem. Commun.* 8, 18–21. doi: 10.1016/j.inoche.2004.10.021

Gao, R.-C., Guo, F.-S., Bai, N.-N., Wu, Y.-L., Yang, F., Liang, J.-Y., et al. (2016). Two 3D Isostructural Ln(III)-MOFs: displaying the slow magnetic relaxation and luminescence properties in detection of nitrobenzene and Cr$_2$O$_7^{2-}$, *Inorg. Chem.* 55, 11323–11330. doi: 10.1021/acs.inorgchem.6b01899

Gatteschi, D., and Sessoli, R. (2003). Quantum tunneling of magnetization and related phenomena in molecular materials. *Angew. Chem. Int. Ed.* 42, 268–297. doi: 10.1002/anie.200390099

Ghosh, M. K., Chandraker, S. K., Shukla, R., Mandal, M., Mandal, V., and Ghorai, T. K. (2019a). Molecular interaction, antimicrobial, antioxidant, cytotoxic and magnetic properties of Mn12 benzoate. *J. Cluster Sci.* 31, 575–589. doi: 10.1007/s10876-019-01633-5

Ghosh, M. K., Pathak, S., and Ghorai, T. K. (2019b). Synthesis of two mononuclear schiff base metal (M= Fe, Cu) complexes: MOF structure, dye degradation, H$_0$O$_2$ sensing, and DNA binding property. *ACS Omega* 4, 16068–16079. doi: 10.1021/acsomega.9b02268

Gupta, S. K., Rajeshkumar, T., Rajaraman, G., and Murugavel, R. (2016). An air-stable Dy (III) single-ion magnet with high anisotropy barrier and blocking temperature. *Chem. Sci.* 7, 5181–5191. doi: 10.1039/C6SC00279J

Ishikawa, N., Sugita, M., Ishikawa, T., Koshihara, S. Y., and Kaizu, Y. (2003). Lanthanide double-decker complexes functioning as magnets at the single-molecular level. *J. Am. Chem. Soc.* 125, 8694–8695. doi: 10.1021/ja029629n

King, P., Wernsdorfer, W., Abboud, K. A., and Christou, G. (2005). Single-molecule magnets: a reductive aggregation route to new types of Mn12 complexes. *Inorg.Chem.* 44, 8659–8669. doi: 10.1021/ic051150j

Koo, Won-Tae., Choi, Seon-Jin., Kim, Sang-Joon., Jang, Ji-Soo., and Tuller, H. L.;, Kim, Il-Doo. (2016). Heterogeneous sensitization of metal–organic framework driven metal@metal oxide complex catalysts on an oxide nanofiber scaffold toward superior gas sensors, *J. Am. Chem. Soc.* 138, 13431–13437. doi: 10.1021/jacs.6b09167

Kumar, K., Stefańczyk, O., Chorazy, S., Nakabayashi, K., Sieklucka, B., Ohkoshi, S.-I. (2019). Effect of noble metals on luminescence and single-molecule magnet behavior in the cyanido-bridged Ln–Ag and Ln–Au (Ln = Dy, Yb, Er) complexes. *Inorg. Chem.* 58, 5677–5687. doi: 10.1021/acs.inorgchem. 8b03634

Li, H. G., Yang, Z. Y., Wang, B. D., and Wu, J. C. (2010). Synthesis, crystal structure, antioxidation and DNA-binding properties of the Ln complexes with 1-phenyl-3-methyl-5-hydroxypyrazole-4-carbaldhyde-(benzoyl) hydrazone. *J. Organomet. Chem.* 695, 415–422. doi: 10.1016/j.jorganchem.2009.10.032

Long, J. (2019). Luminescent schiff-base lanthanide single-molecule magnets: the association betweeen optical and magnetic properties. *Front. Chem.* 7:63. doi: 10.3389/fchem.2019.00063

Lv, J., Liu, T., Cai, S., Wang, X., Liu, L., and Wang, Y. (2006). Synthesis, structure and biological activity of cobalt (II) and copper (II) complexes of valine-derived schiff bases. *J. Inorg. Biochem.* 100, 1888–1896. doi: 10.1016/j.jinorgbio.2006.07.014

Mandal, A., Dasgupta, S., Ganguly, S., Bauzá, A.,Frontera, A., and Das, D. (2017). Cooperative influence of pseudohalides and ligand backbone of Schiff-bases on nuclearity and stereochemistry of cobalt (III) complexes: experimental and theoretical investigation. *Dalton Trans.* 46, 15257–15268. doi: 10.1039/C7DT03040A

Modak, R., Sikdar, Y., Thuijs, A. E., Christou, G., and Goswami, S. (2016). CoII4, CoII7, and a series of CoII2LnIII (LnIII= NdIII, SmIII, GdIII, TbIII, DyIII) coordination clusters: search for single molecule magnets. *Inorg. Chem.* 55, 10192–10202. doi: 10.1021/acs.inorgchem.6b01402

Montgomery, C. P., Murray, B. S., New, E. J., Pal, R., and Parker, D. (2009). Cell-penetrating metal complex optical probes: targeted and responsive systems based on lanthanide luminescence. *Acc. Chem. Res.* 42, 925–937. doi: 10.1021/ar800174z

Pages, B. J., Ang, D. L., Wright, E. P., and Aldrich-Wright, J. R. (2015). Metal complex interactions with DNA. *Dalton Trans.* 44, 3505–3526. doi: 10.1039/C4DT02700K

Patel, M. N., Gandhi, D. S., and Parmar, P. A. (2011). Synthesis, biological aspects and SOD mimic activity of square pyramidal copper (II) complexes with the 3rd generation quinolone drug sparfloxacin and phenanthroline derivatives. *Inorg. Chem. Commun.* 14, 128–132. doi: 10.1016/j.inoche.2010.10.003

Pathak, S., Ghosh, M. K., and Ghorai, T. K. (2018). Luminescence, dye degradation and DNA binding properties of a dinuclear nona-coordinated Y (III) complex. *Chem. Select.* 3, 13501–13506. doi: 10.1002/slct.201801826

Pathak, S.,Ghosh, M. K.,Mandal, M., Mandal, V., Bhattacharyya, A., and Ghorai, T. K. (2019). Synthesis of a new acetate bridged Cu (ii) building block generated 1D polymer and studies on structural, magnetic, antibacterial and anticancer properties. *New J. Chem.* 43, 2019–2029. doi: 10.1039/C8NJ04937H

Qi, X., Tian, H., Dang, X., Fan, Y., Zhanga and Huimin Zhao (2019). A bimetallic Co/Mn metal–organic-framework with a synergistic catalytic effect as peroxidase for the colorimetric detection of H$_2$O$_2$. *Anal. Methods* 11, 1111–1124. doi: 10.1039/C.8A. Y.02514B

Santini, C., Pellei, M., Gandin, V., Porchia, M., Tisato, F., and Marzano, C. (2013). Advances in copper complexes as anticancer agents. *Chem. Rev.* 114, 815–862. doi: 10.1021/cr400135x

Sengupta, S. K., Pandey, O. P., Srivastava, B. K., and Sharma, V. K. (1998). Synthesis, structural and biochemical aspects of titanocene and zirconocene chelates of acetylferrocenylthiosemicarbazones. *Transition Met. Chem.* 23, 349–353. doi: 10.1023/A:1006986131435

Sessoli, R., Gatteschi, D., Caneschi, A., and Novak, M. A. (1993a). Magnetic bistability in a metal-ion cluster. *Nature* 365:141. doi: 10.1038/365141a0

Shahabadi, N., Kashanian, S., and Darabi, F. (2010). DNA binding and DNA cleavage studies of a water soluble cobalt (II) complex containing dinitrogen Schiff base ligand: the effect of metal on the mode of binding. *Eur. J. Med. Chem.* 45, 4239–4245. doi: 10.1016/j.ejmech.2010.06.020

Sheldrick, G. M. (1996). *2010 SADABS*. Göttingen: University of Göttingen.

Sheldrick, G. M. (2008). A short history of SHELX. *ActaCrystallogr. Sec. A.* 64,112–122. doi: 10.1107/S0108767307043930

Sheldrick, G. M. (2013). *ShelXL2013*. Germany: University of Göttingen.

Tang, J., and Zhang, P. (2015). *Lanthanide Single Molecule Magnets*, Berlin: Springer. 41-90. doi: 10.1007/978-3-662-46999-6_2

Tasiopoulos, A. J., Vinslava, A., Wernsdorfer, W., Abboud, K. A., and Christou, G. (2004). Giant single-molecule magnets: a {Mn84} torus and its supramolecular nanotubes. *Angew. Chem. Int. Ed.* 43, 2117–2121. doi: 10.1002/anie.200 353352

Tredwin, C. J., Naik, S., Lewis, N. J., and Scully, C. B. E. C. (2006). Hydrogen peroxide tooth-whitening (bleaching) products: review of adverse effects and safety issues. *Br. Dent. J.* 200, 371–376. doi: 10.1038/sj.bdj.4813423

Turan, N., Gündüz, B., Körkoca, H., Adigüzel, R., and Çolak, N., Buldurun, K. (2014). Study of structure and spectral characteristics of the Zinc (II) and Copper (II) complexes with 5, 5-Dimethyl-2-(2-(3-nitrophenyl) hydrazono) cyclohexane-1, 3-dione and their effects on optical properties and the developing of the energy band gap and investigation of antibacterial activity. *J. Mex. Chem. Soc.* 58, 65–75.

Van Slageren, J. (2011). "New directions in electron paramagnetic resonance spectroscopy on molecular nanomagnets," in *EPR spectroscopy* (Berlin: Springer) 199–234. doi: 10.1007/128_2011_303

Vincent, R., Klyatskaya, S., Ruben, M., Wernsdorfer, W., and Balestro, F. (2012). Electronic read-out of a single nuclear spin using a molecular spin transistor. *Nature* 488:357. doi: 10.1038/nature11341

Wang, B. D., Yang, Z. Y., Wang, Q., Cai, T. K., and Crewdson, P. (2006). Synthesis, characterization, cytotoxic activities, and DNA-binding properties of the La (III) complex with Naringenin Schiff-base. *Bioorg. Med. Chem.* 14, 1880–1888. doi: 10.1016/j.bmc.2005.10.031

Wang, J., Liu, X., Sun, Y., Yan, L., and He, S. (2011). Synthesis, crystal structures, thermal properties, and DNA-binding studies of transition metal complexes with imidazole ligands. *J. Coord. Chem.* 64, 1554–1565. doi: 10.1080/00958972.2011.575937

Wang, Q., Huang, Y., Zhang, J. S., and Yang, X. B. (2014). Synthesis, characterization, DNA interaction, and antitumor activities of La (III) complex with Schiff base ligand derived from kaempferol and diethylenetriamine. *Bioinorg. Chem. Appl.* 2014:354138. doi: 10.1155/2014/354138

Weast, R. C., and Astle, M. J. (1984). *CRC Handbook of Chemistry and Physics, 64 Edn.* Boca Raton, FL: CRC.

Wolfe, A., Shimer, G. H. Jr, and Meehan, T. (1987). Polycyclic aromatic hydrocarbons physically intercalate into duplex regions of denatured DNA. *Biochemistry* 26, 6392–6396. doi: 10.1021/bi00394a013

Woodruff, D. N., Winpenny, R. E., and Layfield, R. A. (2013). Lanthanide single-molecule magnets. *Chem. Rev.* 113, 5110–5148. doi: 10.1021/cr400018q

Wu, D. F., Liu, Z., Ren, P., Liu, X. H., Wang, N., Cui, J. Z., et al. (2019). A new family of dinuclear lanthanide complexes constructed from an 8-hydroxyquinoline Schiff base and β-diketone: magnetic properties and near-infrared luminescence. *Dalton Trans.* 48, 1392-1403, (b) Tang, Y., Feng, Y., Gan, X., Tan, M., Yu, K. (1996). Preparation and structure of [bis (8-quinolyloxyethyl)ether· H$_{3+}$O]$_3$[La(NO$_3$)$_6$]: A hexanitrato lanthanum complex of a hydronium ion podand complex cation. *Polyhedron* (1996). 15, 3219–3223. doi: 10.1039/C8DT04384A

Yang, L., Xu, C., Ye, W., and Liu, W. (2015). An electrochemical sensor for H$_2$O$_2$ based on a new Co-metal-organic framework modified electrode. *Sens. Actuators B Chem.* 215, 489–496. doi: 10.1016/j.snb.2015.03.104

Yang, Z. Y., Wang, B. D., and Li, Y. H. (2006). Study on DNA-binding properties and cytotoxicity in L1210 of La (III) complex with PMBP-isonicotinoylhydrazone. *J. Organomet. Chem.* 691, 4159–4166. doi: 10.1016/j.jorganchem.2006.06.002

Yang, Z. Y., Yang, R. D., Li, F. S., and Yu, K. B. (2000). Crystal structure and antitumor activity of some rare earth metal complexes with Schiff base. *Polyhedron* 19, 2599–2604. doi: 10.1016/S0277-5387(00)00562-3

Yuan, S, Qin, J.-S., Lollar, C. T., and Zhou, H.-C. (2018). Stable metal–organic frameworks with group 4 metals: current status and trends. *ACS Cent. Sci.* 4, 440–450. doi: 10.1021/acscentsci.8b00073

Zeng, H. H., Qiu, W. B., Zhang, L., Liang, R. P., and Qiu, J. D. (2016). Lanthanide coordination polymer nanoparticles as an excellent artificial peroxidase for hydrogen peroxide detection. *Anal. Chem.* 88, 6342–6348. doi: 10.1021/acs.analchem.6b00630

Zeng, H. H., Zhang, L., Rong, L. Q., Liang, R. P., and Qiu, J. D. (2017). A luminescent lanthanide coordination polymer based on energy transfer from metal to metal for hydrogen peroxide detection. *Biosens. Bioelectron.* 89, 721–727. doi: 10.1016/j.bios.2016.11.020

Zhang, T., Manna, K., and Lin, W. (2016). Metal–organic frameworks stabilize solution-inaccessible cobalt catalysts for highly efficient broad-scope organic transformations. *J. Am. Chem. Soc.* 138, 3241–3249. doi: 10.1021/jacs.6b00849

Zhao, W., Wang, Z., and Li, Q. (2012). Fabrication of a nichrome electrode coated with silver microcrystals, and its application to sensing hydrogen peroxide. *Anal. Methods.* 4, 1105–1109. doi: 10.1039/c2ay05904e

Zuber, G., Quada, J. C., and Hecht, S. M. (1998). Sequence selective cleavage of a DNA octanucleotide by chlorinated bithiazoles and bleomycins. *J. Am. Chem. Soc.* 120, 9368–9369. doi: 10.1021/ja981937r